Earthquakes and Structures, *Vol. 8, No. 6 (2015) 1277-1297*
DOI: http://dx.doi.org/10.12989/eas.2015.8.6.1277

Evaluating seismic demands for segmental columns with low energy dissipation capacity

Ehsan Nikbakht*, Khalim Rashid[a], Iman Mohseni[b] and Farzad Hejazi[b]

Department of Civil and Structural Engineering, Universiti Kebangsaan Malaysia, 43600 Bangi, Malaysia

(Received December 1, 2013, Revised November 14, 2014, Accepted November 14, 2014)

Abstract. Post-tensioned precast segmental bridge columns have shown high level of strength and ductility, and low residual displacement, which makes them suffer minor damage after earthquake loading; however, there is still lack of confidence on their lateral response against severe seismic loading due in part to their low energy dissipation capacity. This study investigates the influence of major design factors such as post-tensioning force level, strands position, columns aspect ratio, steel jacket and mild steel ratio on seismic performance of self-centring segmental bridge columns in terms of lateral strength, residual displacement and lateral peak displacement. Seismic analyses show that increasing the continuous mild steel ratio improves the lateral peak displacement of the self-centring columns at different levels of post-tensioning (PT) forces. Such an increase in steel ratio reduces the residual drift in segmental columns with higher aspect ratio more considerably. Suggestions are proposed for the design of self-centring segmental columns with various aspect ratios at different target drifts.

Keywords: post-tensioning; precast segmental columns; earthquake loading; finite element method (FEM); lateral seismic demand; residual displacement

1. Introduction

Precast segmental bridge columns have been a popular subject of many researchers in recent years. The reason for this interest is due to their appropriate performance against severe earthquakes, where they remain functional and repairable with lower amount of cracks and damage. Moreover, the ease of construction of prefabricated segmental columns makes it possible to construct them to a higher quality. Precast segmental bridge columns react against earthquake loading with a rocking action. Fig. 1 illustrates the behaviour of precast segmental columns' segmental rocking action against lateral seismic loading. The uplifting of segments prevents the formation of a plastic hinge at the base of the column. In comparison with conventional cast-in-place RC bridge columns, they face a lower amount of damage after severe earthquakes. The precast hybrid post-tensioned bridge components are composed of energy dissipating bars and post-tensioned tendons, which have a flag-shaped hysteretic performance against seismic loading.

*Corresponding author, E-mail: enikbakht@siswa.ukm.edu.my
[a]Associate Professor
[b]Ph.D.

http://www.techno-press.org/journals/eas&subpage=7 ISSN: 2092-7614 (Print), 2092-7622 (Online)

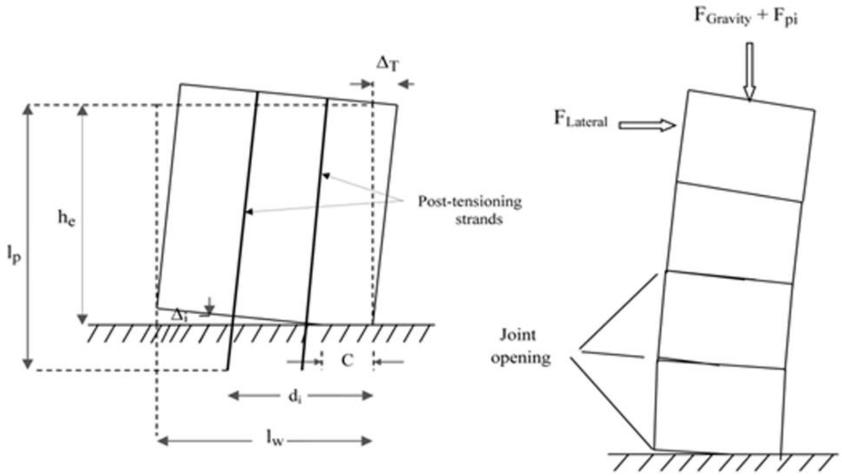

Fig. 1 Uplifting of segments in precast segmental columns against lateral loading

To date, investigations have focused on various hybrid post-tensioned seismic structures, including frames and shear walls (Stone *et al*. 1995, Stanton *et al*. 1998). In these studies, hybrid post-tensioned frames were applied to demonstrate how a combination of PT strands and mild steel bars perform appropriately against seismic loading with negligible residual displacement.

The unbonded post-tensioned systems are advantageous in delaying the yielding of PT strands, because the induced stresses are distributed throughout the strands, while energy dissipation remains low in comparison to the bonded post-tensioned columns. Unbonded and bonded post-tensioned segmental bridge columns have been experimentally and analytically investigated over the past few years. Some of experiments can be found in Hewes and Priestley (2002), Ou-Chen *et al*. (2010), Elgawady *et al*. (2012), Kim *et al*. (2010).

The incompatibility of PT strands and concrete in sectional analysis makes the analytical procedure of precast hybrid post-tensioned columns more complicated. Hewes and Priestley (2002), in using a “monolithic beam analogy” concept, and assuming that major segment opening occurs at the junction of the footing and first column segment, proposed a method for predicting the pushover lateral force-deflection of segmental columns with discontinuous mild steel bars through the joints. Kwan and Billington (2003) proposed some criteria for the functionality and survival limits of precast post-tensioned columns. Ou-Chen *et al*. (2007) extended the previous method, and developed a simplified analytical method for segmental columns with continuous bars and strands. Sakai and Mahin (2004) and Jeong-Il *et al*. (2008) investigated the behaviour of the monolithic self-centring bridge columns. They conducted shaking table tests and analytical methods for the development and validation of the design method for monolithic post-tensioned RC bridge columns against seismic loading. Chou *et al*. (2008) developed a stiffness-degrading flag shape hysteretic model for lateral response of unbonded post-tensioned precast segmental columns. Elgawady and Sha’lan (2011) showed that the precast post-tensioned bridge columns with concrete-filled steel tubes have high ductility and strength, as well as a low level of induced damage and residual displacement. Dawood *et al*. (2012) developed a finite element model for predicting monotonic pushover lateral force-deflection. They investigated the accuracy of the model for predicting the induced damage in this system. More recently, Bu *et al*. (2013) developed a simplified analytical method for pushover analysis of precast segmental columns. In other work, Chue *et al*. (2013) developed two dimensional finite element models for post-tensioned segmental columns.

Despite the appropriate performance of precast post-tensioned bridge columns against seismic loading, there is still a lack of confidence in their application in high seismicity zones. The main concern in this study is to investigate the precast segmental columns with "low energy dissipation capacity". These columns incorporate central post-tensioning strands and there is low contribution of longitudinal mild steel bars in shear strength of the columns. Although these columns have the advantage of low residual displacement against earthquake loading, low energy dissipation capacity in this system may cause undesirable high lateral peak displacement against severe earthquake loading. The present study investigates the seismic demands of such columns in terms of residual displacement and lateral peak displacement. A parametric study is conducted in order to investigate the influence of key parameters such as post-tensioning level, strands position, steel tube jacketing and longitudinal mild steel ratio on this kind of columns at different aspect ratios. Nonlinear static and dynamic time-history analyses are performed to examine and evaluate the upper limits for the energy dissipation capacity of this type of bridge columns while maintaining the residual displacement within the requirement of the standard design codes.

This study also inspects the effect of continuous longitudinal mild steel bars on residual displacement and equivalent viscous damping of the self-centring segmental columns at different target drifts, which can be used in design procedures such as displacement-based approach.

2. Experimental program

A column specimen with an aspect ratio of 4.30 is tested in the laboratory in order to study the performance of these types of bridge columns with continuous mild steel starter bars under earthquake type loading and also to verify the load-deflection response obtained by the numerical method. The geometry of the specimen is shown in Fig. 2. The specimen is a 40% scale model of a circular prototype bridge column, which has a hollow core cross section for allowing passage of unbonded post-tensioning strands. This column is composed of three reinforced concrete segments, a footing foundation and a load stub in precast segment configuration (Fig. 3). All segments are connected together by 19 central unbonded post-tensioning strands with diameter of 12.7 mm. In Table 1, compressive strength of concrete are measured for 1 day, 7 day, 28 day and the day of testing. Also, the yield strength and ultimate strength of mild steel bars and PT strands are listed in Tables 2 and 3.

2.1 Test process

The test set-up is shown in Fig. 4. The specimen is connected to a strong floor in the laboratory by six high tensile studs. The load stub is also connected to a rigid wall by four high tensile studs with the diameter of 32 mm. An actuator with 500 kN and ±100 mm stroke capacity is used for applying lateral loading. Firstly, axial force of 1470 kN is applied as post-tensioning force to the 19 PT strands with 12.7 mm diameter. Seven cycles of lateral loading with amplitude of 0.6%, 0.9%, 1.2%, 1.6%, 2.2%, 3.0% and 4.0% are performed. The loading in pulling direction is eliminated during testing due to the low capacity of the available actuator in the laboratory and also due to the fact that cyclic behaviour of the specimen in both directions are similar since there is a symmetric configuration of reinforcements in the specimen.

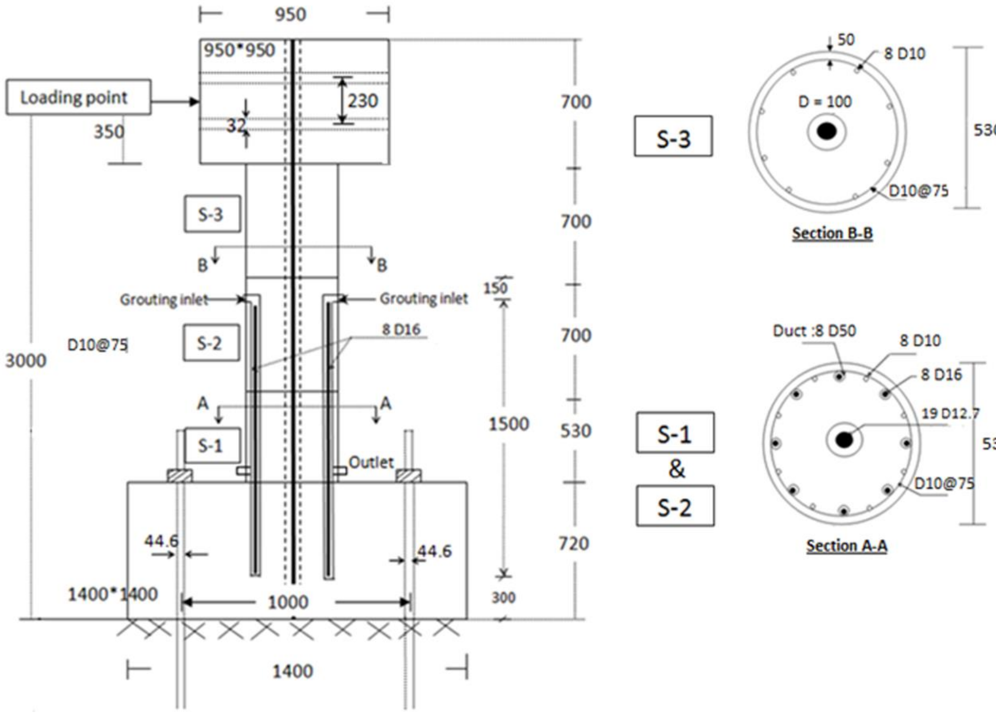

Fig. 2 Dimensions and geometry of the test specimen

Table 1 Compressive strength of concrete applied in the segments, load stub and footing

Specimen	1 day	7 day	28 day	Day of testing
Segment 1	38.2	49	58	70.3
Segment 2	38.6	50	62	73.4
Segment 3	40.0	52	65	75.1
Footing	-	36.3	47.2	58.4
Load stub	-	36.3	47.2	58.4

Table 2 Properties of steel bars used in the specimen

Description	Size	Yield strength (MPa)	Ultimate strength (MPa)
Discontinuous longitudinal bars	12.7 mm	460	730
Anchor spirals	19.1 mm	430	680
Segmental spirals	9.5 mm	460	730
Bonded continuous bars	16.0 mm	460	730

Table 3 Characteristics of the 7-wire used in the specimen

Type of strand	Nominal dia mm	Nominal tensile strength N/mm^2	Nominal steel area mm^2	Nominal mass g/m	Minimum elongation L>500 mm	Relaxation
7-wire strand	12.7	1770	93	730	3.5%	2.5%

Fig. 3 Precast footing, load stub and the segments of the specimen before and after assembling

Fig. 4 Test set-up in the laboratory

2.2 Test results

The force-displacement response of the specimen up to 4.0% drift (90.4 mm) is displaced in Fig. 5. As can be seen in the figure, a significant non-linear behaviour is initiated at a force level of approximately 110 kN. Maximum column strength was achieved at the applied displacement of 85 mm and was 166.3 kN. The column showed relatively low energy dissipation as well as small residual drift (less than 1.0%). The maximum opening of segments during loading occurred at the interface of footing-first segment. At the end of test, flexural cracks formed at the middle of segments one and two. The major amount of segments opening occurred at the interface of footing-first segment as shown in Fig. 6. It is noticed that some minor vertical cracks were formed around the grouting inlet and outlets along with bonded continuous longitudinal reinforcements. The amount of opening at the interface of footing-first segment was approximately 18 mm as shown in Fig. 6. At the drift level of 4.0%, the amount of crack opening at the interface of segment one and segment two was approximately 5.0 mm.

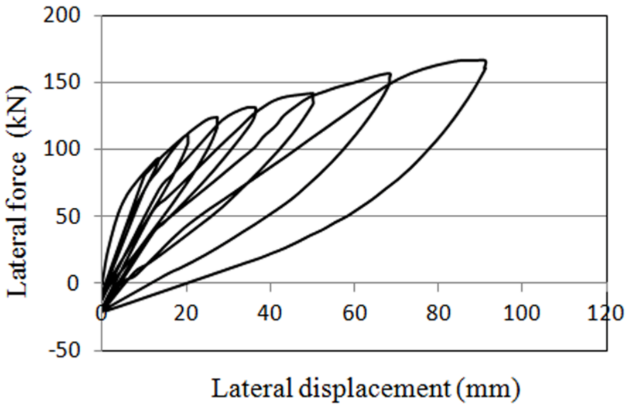

Fig. 5 Lateral load-displacement of the specimen under first testing

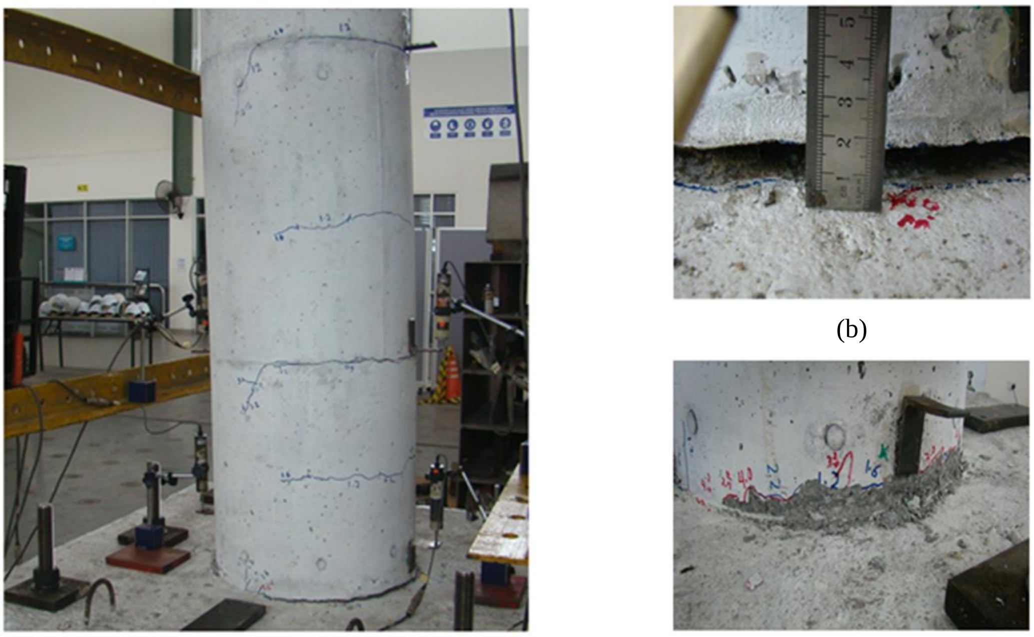

(a) (b) (c)

Fig. 6 Observed behavior of the specimen at 4.0% drift: (a) flexural cracks at the segments one and two (b) opening at the junction of footing-first segment (c) concrete crush induced at the compression toe of the specimen

3. Numerical analysis

In this study, 3D nonlinear finite element ANSYS 13.0 (2012) software is implemented to investigate analytically the behaviour of precast segmental bridge samples against lateral seismic loading. For validation and verification of the analytical model, the numerical results are compared with the experimental results of this study. In this section a model for hybrid post-tensioned segmental column are developed. The details of modelling are illustrated in the following sections.

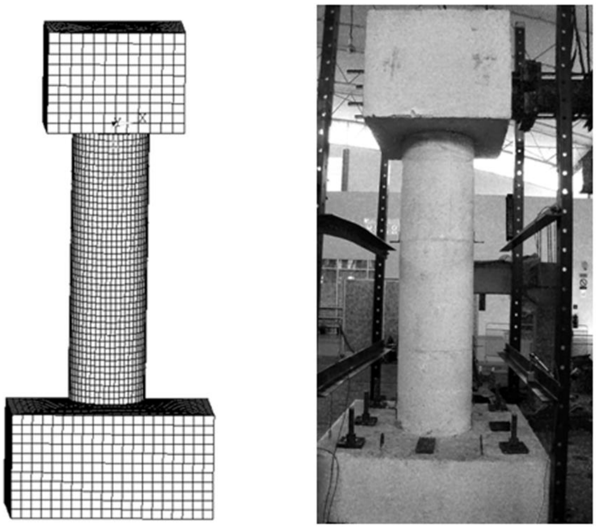

Fig. 7 Mesh configuration for modelling of specimen

3.1 Types of elements and material properties

Fig. 7 shows the geometry and mesh configuration applied for modelling of the specimen. In modelling, the specimen is completely fixed at the bottom of footing. Unbonded central PT strands with total area of 1767 mm^2 are passed through a hollow duct. For modelling of contact between strands (Link 185) and concrete around (Solid 65), elements of Contact174 and Target170 are used. Moreover, there are Contact174 and Target170 elements for modelling the contact between two adjacent segments. In the first step of loading, a prestressing load of 1470 kN are applied in PT strands. In the next step of loading, both ending of PT strands are locked for fixing the prestressing load in strands. Then lateral cyclic loading are imposed. Some necessary parameters for modelling of reinforcements, PT strands, and stress-strain of concrete of segments, footing and load stub are listed in Tables 4 to 6.

3.2 Stress-strain model for concrete, prestressing and mild steel bars

Concrete is a quasi-brittle material that behaves differently under compression and tension. Generally, concrete's tensile strength is only 8% to 15% of the compressive strength. The model developed by Desayi and Krishnan (1964) is used for compressive and tensile stress-strain of concrete. Further information regarding modelling of concrete and other materials which are applied here is referred to the earlier work done by the authors (Nikbakht *et al*. 2014). The ultimate

$$\sigma_{cu} = \left(\frac{E_o}{4700}\right)^2 \tag{1}$$

$$\sigma_{tu} = 0.62\sqrt{\sigma_{cu}} \tag{2}$$

concrete compressive and tensile stress for concrete is in Eqs. (1) and (2).

A non-linear prestressing steel stress strain model according to Caltrans seismic design (1999) is adopted, which can be constructed by Eqs. (3) and (4).

$$\varepsilon_s \leq 0.0086 : f_s = 28{,}500\varepsilon_s \tag{3}$$

$$\varepsilon_s \geq 0.0086 : f_s = 270 - \frac{0.04}{\varepsilon_s - 0.007} \tag{4}$$

Bilinear elastic-perfectly plastic stress-strain has been assumed for the longitudinal and transverse mild steel bars.

Table 4 Necessary parameters for the modelling of PT strands

Post-tensioning strands (Solid185)	
Linear isotropic E_x (N/mm^2)	200,000
Poisson ratio	0.3
Yield stress (MPa)	1780

Table 5 Necessary parameters for bilinear isotropic modelling of reinforcements

Ø 10 (Link 8)	
Linear isotropic E_x (N/mm^2)	200,000
Poisson ratio	0.3
Yield stress (MPa)	430
Ø 12.7 (Link 8)	
Linear isotropic E_x (N/mm^2)	200,000
Poisson ratio	0.3
Yield stress (MPa)	460
Ø 16.0 (Link 8)	
Linear isotropic E_x (N/mm^2)	200,000
Poisson ratio	0.3
Yield stress (MPa)	460

Table 6 Necessary parameters for multilinear isotropic modelling of concrete for the segments, footing and load stub

Concrete for segments		Concrete for footing and load stub	
Strain	Stress	Strain	Stress
0.00053	21.0	0.00046	15.60
0.0008	29.9	0.00065	21.08
0.0010	36.4	0.00085	26.75
0.0016	52.3	0.0012	35.27
0.0022	62.6	0.0021	48.47
0.0030	68.9	0.0028	51.78
0.00356	70.0	0.0030	52.0

3.3 Numerical results

The results of load-displacement response computed by FEM are compared with the experimental results in Fig. 8. As shown in the figure, there is a good agreement between numerical method and experimental results. The figure indicates that there is slightly higher stiffness for the model during first cycles in FEM compared to the experimental response; however, at 4.0% drift level this difference is less than 5.0%, which implies the accuracy of the numerical method. In Fig. 9, the stress distribution of the specimen at 4.0% drift level in FEM is compared with the concrete crush induced to the specimen, which both FEM and the experimental test the maximum stress occurred at the base of column at the interface of footing-first segment. Furthermore, the base opening of the model obtained by FEM is shown in Fig. 10, which is in good agreement with experiment.

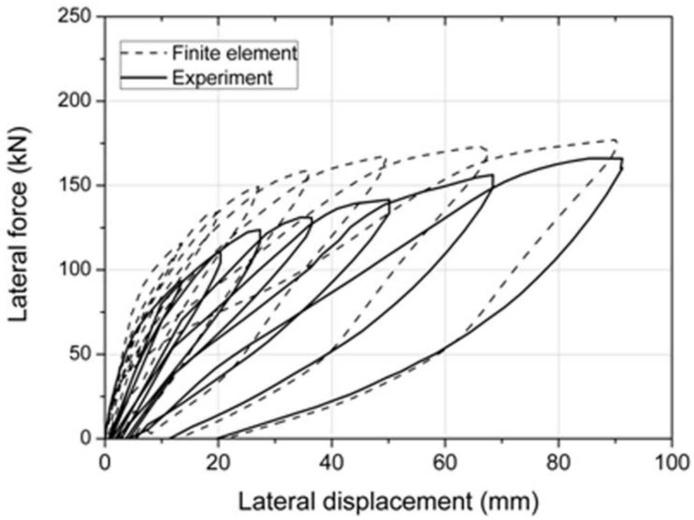

Fig. 8 Lateral load-displacement response of specimen in FEM and experiment

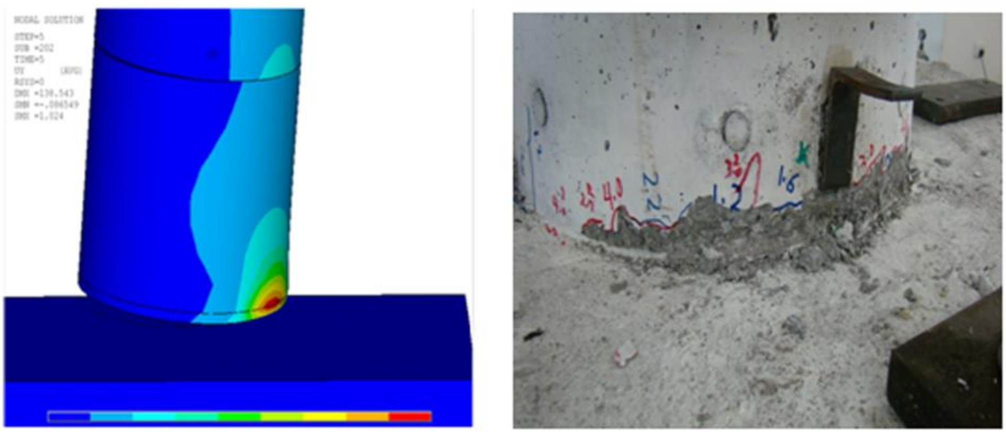
Fig. 9 Distribution of stress in FEM and concrete crush in experiment

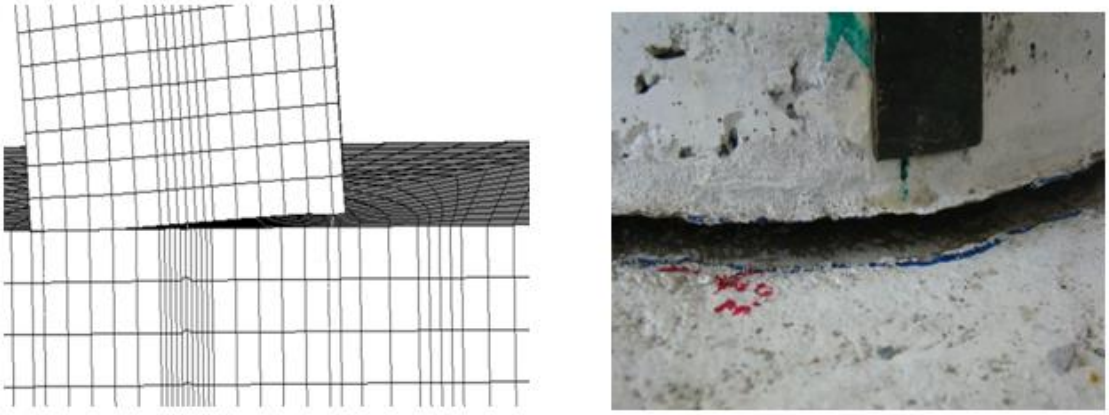

Fig. 10 Column base opening in FEM and experiment

4. Comparison with the models tested by Hewes and Priestley (2002)

In this section, for further validation of numerical method, two unbonded post-tensioned segmental columns with aspect ratios of 3.0, and 6.0, tested by Hewes and Priestley (2002), are modelled. The geometry and dimensions of the segmental columns are shown in Fig. 11. There are central PT strands with a total area of 2665 mm^2 and axial force equivalent of 40% yielding stress of strands. The column with a high aspect ratio is composed of four segments. Steel tube jacketing with a 6.0 mm diameter is around the first segment, which starts 25 mm above the footing so as to avoid the premature failure of concrete at the junction of the footing-first segment. There are two segments in the low aspect ratio column. The thickness of the steel tube jacketing in this sample is 3.0 mm. The material properties of the columns are summarised in Table 7. In Figs. 12 and 13 the hysteretic lateral response of both columns with aspect ratios of 6.0 and 3.0 calculated by the finite element method (FEM) are compared with the experimental results. These figures indicate that both precast segmental columns exhibit negligible residual displacement due to the restoration capability of the central strands. As can be seen in Fig. 12(a), there is a concurrence between the analytical and experimental results for lateral cyclic loading-displacement response of the high aspect ratio column (aspect ratio=6.0) and the stiffness, strength, residual displacement and energy dissipation capacity obtained by the FEM closely follow the experimental results. The formation of concrete cracks and crushing in this column is also captured appropriately by the analytical method.

The analytical results of stiffness, strength and residual displacement of the low aspect ratio column (aspect ratio=3.0) shown in Fig. 13(a), and also the joint opening of the footing-first segment of this column (Fig. 13(b)) are in good agreement with the experimental results. The reason for the slight difference of unloading path between experimental and analytical method in Fig. 13(a) is that this unit column has very short length. According to the experimental report, in order to achieve the design prestress force in this specimen, which has short length of unbonded tendon, the applied post-tensioning force exceeded the prestressing steel limit of proportionality because of the occurrence of significant strain losses as a result of mechanical seating of the strand wedges in the anchor head. However, in this study, the longer columns with aspect ratios of 4.5, 6.0, 7.5 and 9.0 are included and studied.

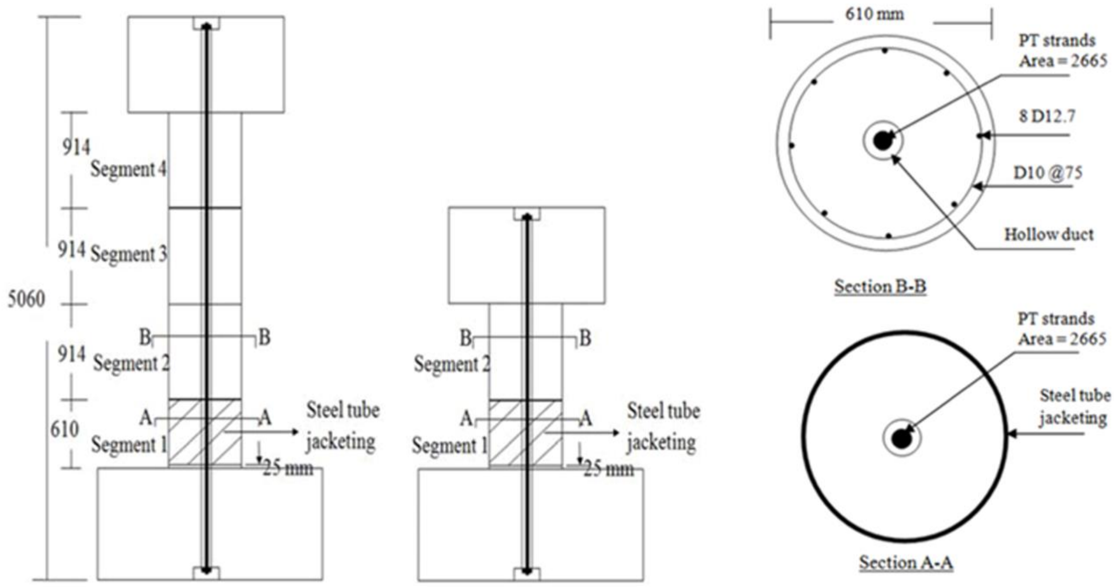

(a) (b)

Fig. 11 Dimension and geometry of precast segmental columns with aspect ratios of (a) 6.0 and (b) 3.0

Table 7 Material properties of the segmental columns tested by Hewes and Priestley (2002)

Material	Numbers	Initial stress (MPa)	Yielding stress(MPa)	Strength (MPa)
Longitudinal reinforcement	8D12.7	-	410	-
Prestressing steel	27D12.7	756	1890	-
Transvers spirals	D10@75	-	410	-
Steel tube jacketing	t=6 (high aspect ratio) t=3 (low aspect ratio)	-	317 317	- -
Concrete	-	-	-	41.4

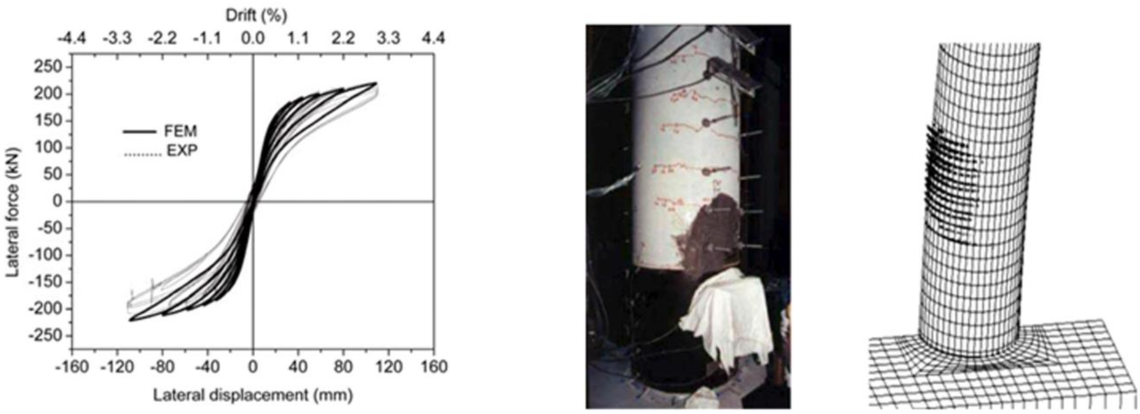

(a) (b)

Fig. 12 Comparison of FEM with the experiment (Hewes and Priestley 2002): sample with aspect ratio of 6

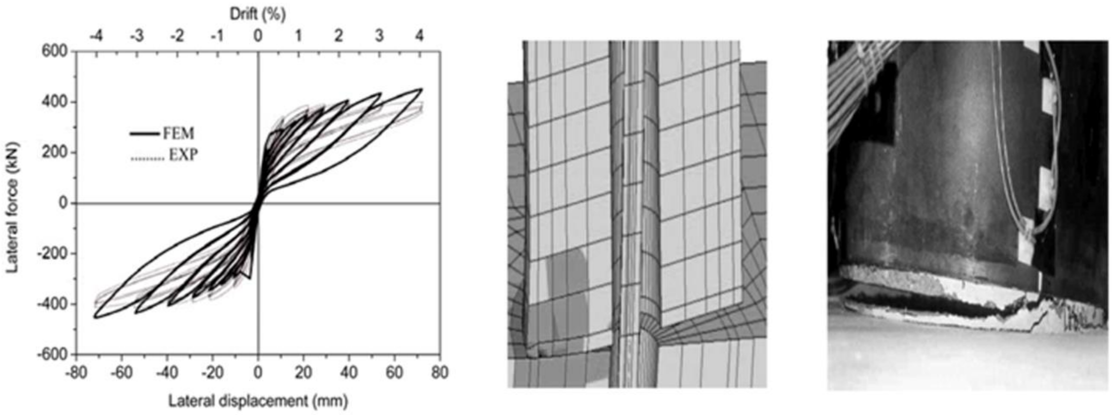

(a) (b)

Fig. 13 Comparison of FEM and experiment (Hewes and Priestley 2002): sample with aspect ratio of 3

5. Parametric study

The effect of parameters such as strand position, post-tensioning force level, steel tube jacketing thickness and mild steel ratio are investigated on seismic behaviour of self-centring segmental columns with low energy dissipation capacity and negligible residual displacement.

5.1 Influence of strand position

In order to investigate the role of strand position on lateral load-carrying capacity, energy dissipation and residual displacement, precast segmental columns with different arrangements of PT strands are analysed and compared with self-centring segmental columns with central PT strands. Fig. 14 shows two segmental columns: one with a 200 mm distance from the centre, and one with 140 mm. The total area of the strands in all columns is 2665 mm^2. In order to provide higher energy dissipation, strands are bonded post-tensioning.

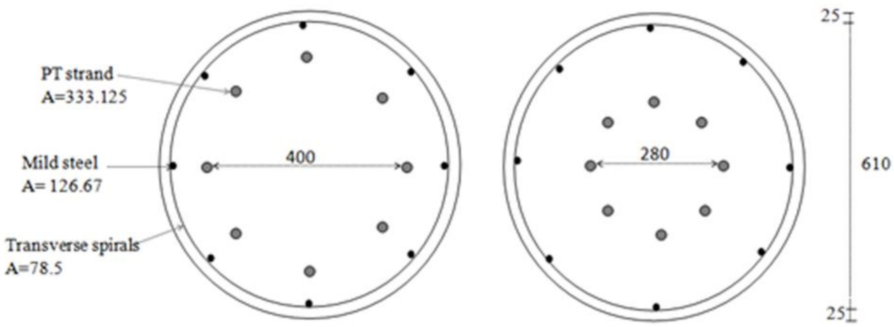

(a) BS400 (b) BS280

Fig. 14 Cross-sections of precast segmental columns with different strand positions

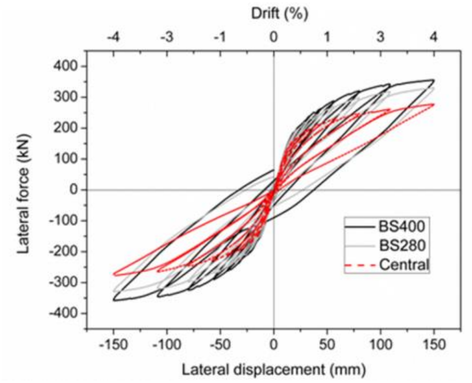

Fig. 15 Lateral response of precast segmental columns with different PT strand positions

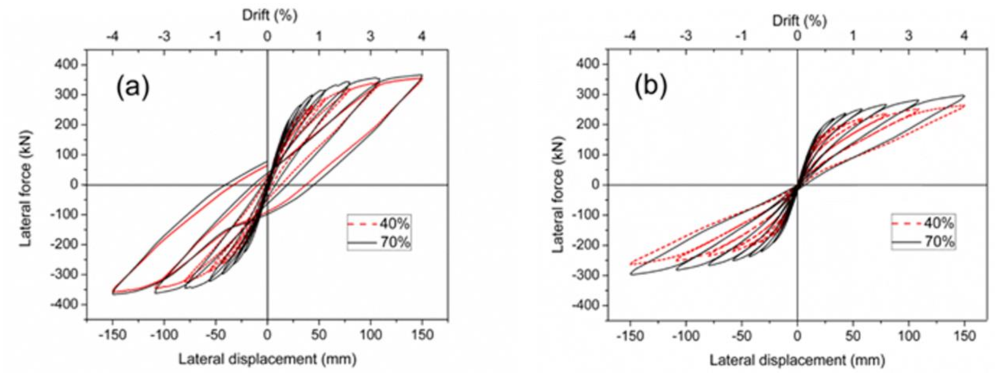

Fig. 16 Lateral response of the segmental columns under 40% and 70% prestressing level: (a) BS400 and (b) the sample with central PT strands

Fig. 15 compares the lateral response of columns with a 400 mm distance between strands (BS400), a 280 mm distance (BS280) and the segmental column with central-bonded PT strands (which is explained in the previous section). The figure indicates that placing strands towards the circumference leads to higher strength compared to columns with strands at the centre, but there is also higher residual displacement. Although the columns with strands placed near the circumference have the advantage of providing higher energy dissipation capacity, they increase the lateral strength of the columns, which requires designing the other bridge components (e.g., decks) stronger as well. There is another disadvantage: higher strength may cause concrete failure in the hinge area of the columns due to excess concrete failure stress. However, the higher energy dissipation leads to more appropriate lateral performance, with lower lateral peak displacement against severe earthquake loading.

In order to investigate the effect of the post-tensioning force level, two segmental columns with different position of strands, i.e., the BS400 sample and the column with central PT strands are analysed and compared under 40% and 70% initial stress levels in Figs. 16(a) and 16(b), respectively. As is shown in the figure, the higher initial stress level (70%) in both types of columns causes the higher initial stiffness. However, the BS400 sample at the 40% initial stress level shows close lateral strength compared with a 70% initial stress level up to 4% drift level. In Fig. 16(b), the ultimate lateral strength difference in central post-tensioned columns is more

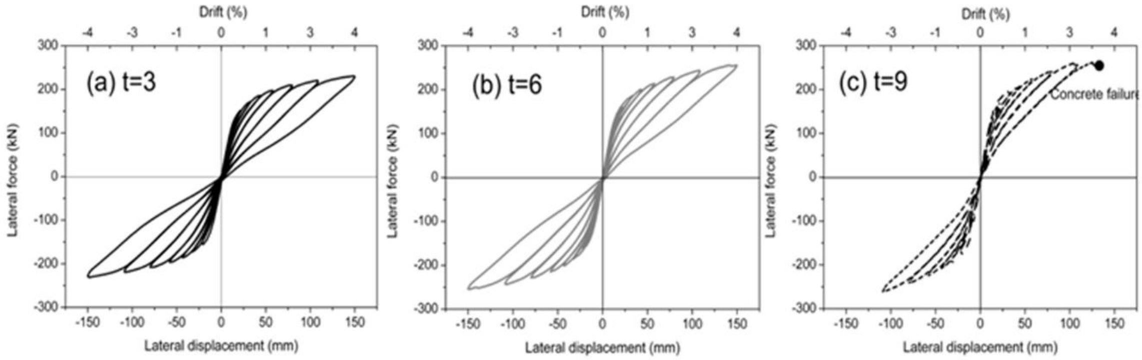

Fig. 17 Lateral response of segmental columns with steel tubes with diameters of 3, 6 and 9 mm around the first segment

pronounced (261 kN strength under 40% initial stress level versus 293 kN strength at 70% initial stress level). The results show that increasing the PT force level has little effect on the residual displacement and energy dissipation capacity of the columns.

5.2 Influence of steel tube jacketing thickness

In this study, steel tube jacketing thickness is investigated as another parameter. Fig. 17 compares the lateral response of the aforementioned precast segmental columns against central PT strands with a thickness of 3, 6 and 9 mm around the first segment. The figure indicates that increasing the thickness of the steel tube slightly increases the stiffness and strength of the column. Columns with a thickness of 3 mm show a strength of 223 kN versus a 275 kN strength for the column with a tube jacketing thickness of 9 mm. In Fig. 17(c), the segmental columns with a tube jacketing thickness of 9 mm fails at 3.6% drift due to concrete failure below the tube jacketing at the joint of the footing-first segment area. In fact, the large thickness of tube jacketing transfers the stress induced in the first segment’s hinge area to the junctions of the footing-first segment; as a consequence, concrete in this area fails.

The results show that the residual displacement and energy dissipation capacity of the columns with central PT strands are not affected by the thickness of the steel tube jacketing.

5.3 Influence of aspect ratio (As) of columns

The lateral response of precast segmental columns with different aspect ratios are compared in Fig. 18. As is shown in the figure, the lateral strength of the columns decreases when the aspect ratio increases. Fig. 19 compares the equivalent viscous damping of the self-centring segmental columns at aspect ratios of 6, 7.5 and 9. The figure indicates that equivalent viscous damping of the columns are not affected by aspect ratio, as they show very close response behaviour. Residual displacement in all columns are negligible. According to Priestley *et al*. (1997) equivalent viscous damping is defined in Eqs. (5) and (6).

$$\xi_{eq}(\%) = \frac{A_h}{4\pi A_e} \tag{5}$$

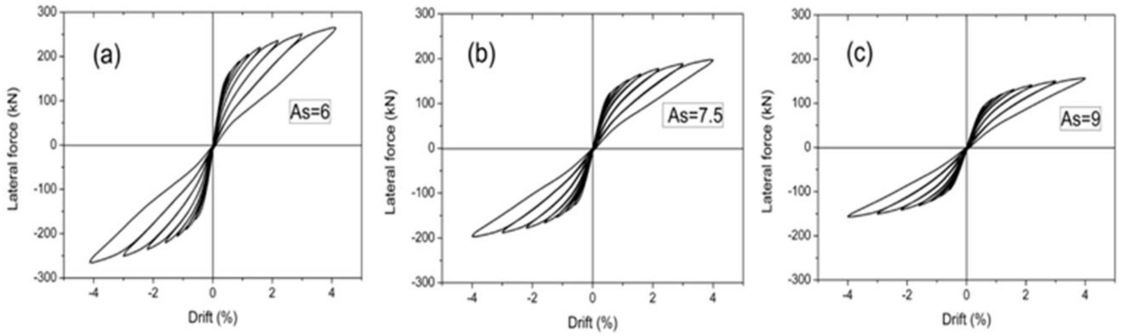

Fig. 18 Lateral response of segmental columns with an aspect ratio of (a) 6, (b) 7.5 and (c) 9

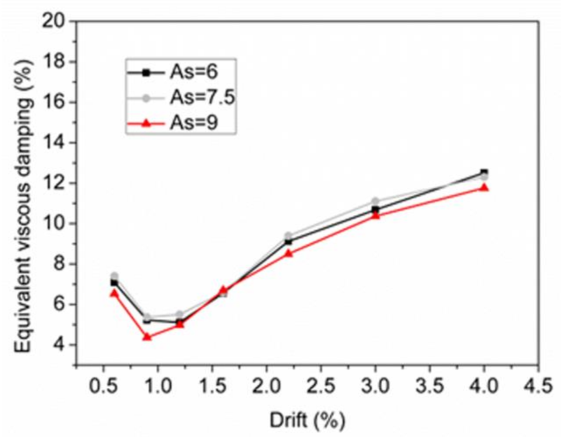

Fig. 19 Equivalent viscous damping of self-centring columns at aspect ratios of 6, 7.5 and 9

$$A_e = \frac{D(P_{\text{Max}} + P_{\text{Min}})}{4} \tag{6}$$

where; A_h is the area enclosed by each cycle; A_e is the elastic energy dissipation; P_{Max} is the lateral load in the push direction, and P_{Min} is the maximum lateral load in the pull direction in each drift; and D is the relevant displacement at the maximum lateral loading point.

5.4 Influence of continuous mild steel ratio

It is shown that self-centring precast segmental columns possess high levels of ductility and strength against seismic loading, and also display negligible residual displacement. However, they have low energy dissipation capacity against severe lateral seismic loading, which leads to large lateral seismic demand.

In order to increase the energy dissipation of the self-centring segmental columns, continuous longitudinal reinforcements are introduced through the joints of the segments. Fig. 20 compares the lateral cyclic response of the precast column with an aspect ratio of 6.0 against various mild steel ratios. As is shown in the figure, by increasing the mild steel ratio, the strength and energy dissipation capacity increases. The residual displacement also increases such that the segmental

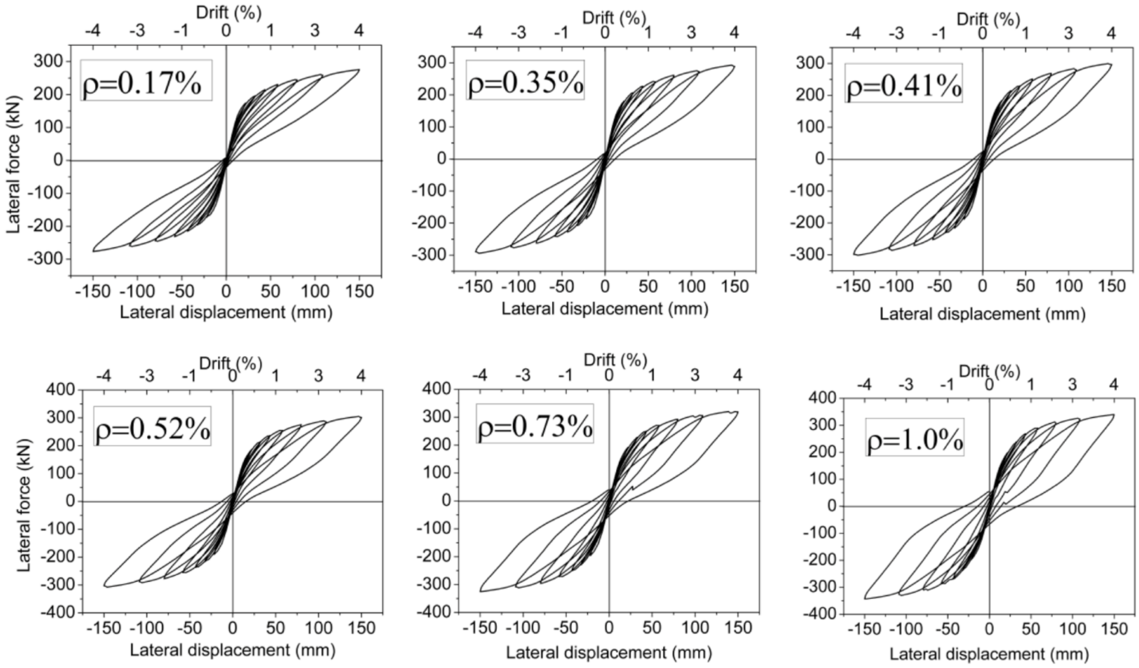

Fig. 20 The effect of the mild steel ratio on the lateral response of self-centring segmental columns with an aspect ratio of 6

column with ρ=0.17% shows negligible residual drift against 1.0% residual drift of the column with ρ=1.0%.

Fig. 21 shows the effect the mild steel ratio has on residual drift of segmental columns with aspect ratios of 4.5, 6, 7.5 and 9. The results are presented for 3.0% and 4.0% drift, as the main residual displacement occurs in these drifts. The figure indicates that the columns with higher aspect ratios show lower residual drift. For instance, in 3.0% drift with a 1.6% mild steel ratio, the column with an aspect ratio of 4.5 has 0.69% residual drift versus 0.43% residual drift for the column with an aspect ratio of 9. According to the Japanese standard codes (2002), 1% residual drift is the limitation for residual drift; any larger than this and it is considered a functionality failure.

At 4.0% target drift, the segmental column with aspect ratio of 4.5 fails due to concrete crush when it has 0.52% steel ratio. The reason for the concrete failure in this sample is that the raising of the mild steel ratio increases initial stiffness and strength, and the stress induced exceeds the failure stress of concrete in the hinge area. The columns with aspect ratios of 6.0, 7.5 and 9.0 fail due to exceeding 1% residual drift when the mild steel ratio is 1.0%, 1.3% and 1.6% respectively. The column with aspect ratio of 6.0 reaches 1% residual drift when it has 1% ratio of mild steel. However, the columns with aspect ratios of 7.5 and 9.0 reach to 1% residual drift when they possess 1.5% and 1.63% mild steel ratios respectively. Fig. 22 compares the effect of mild steel ratio on equivalent viscous damping of segmental columns with different aspect ratios at 1.6%, 3.0% and 4.0% drift levels. As it can be observed from the figure, equivalent viscous damping of all columns increases when the mild steel ratio is raised. The column with the higher aspect ratio shows lower equivalent viscous damping at every drift levels.

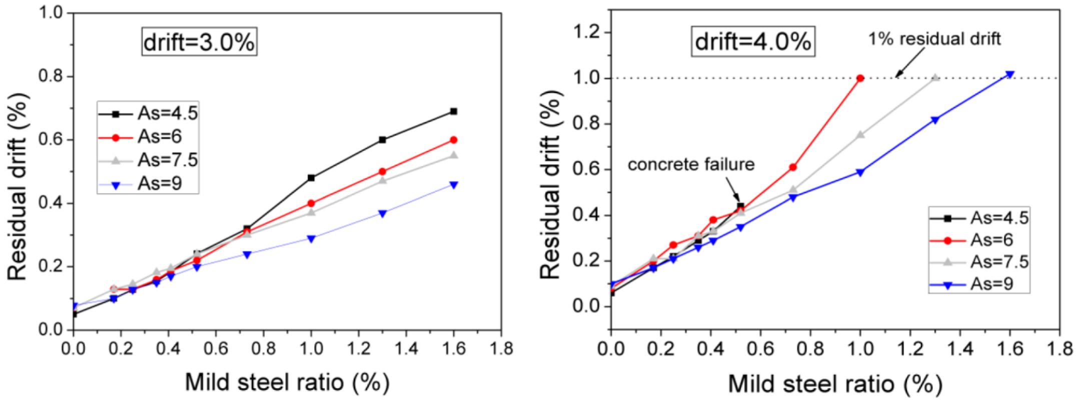

Fig. 21 Effect of mild steel ratio on residual drift of precast segmental columns with various aspect ratios of 4.5, 6, 7.5 and 9

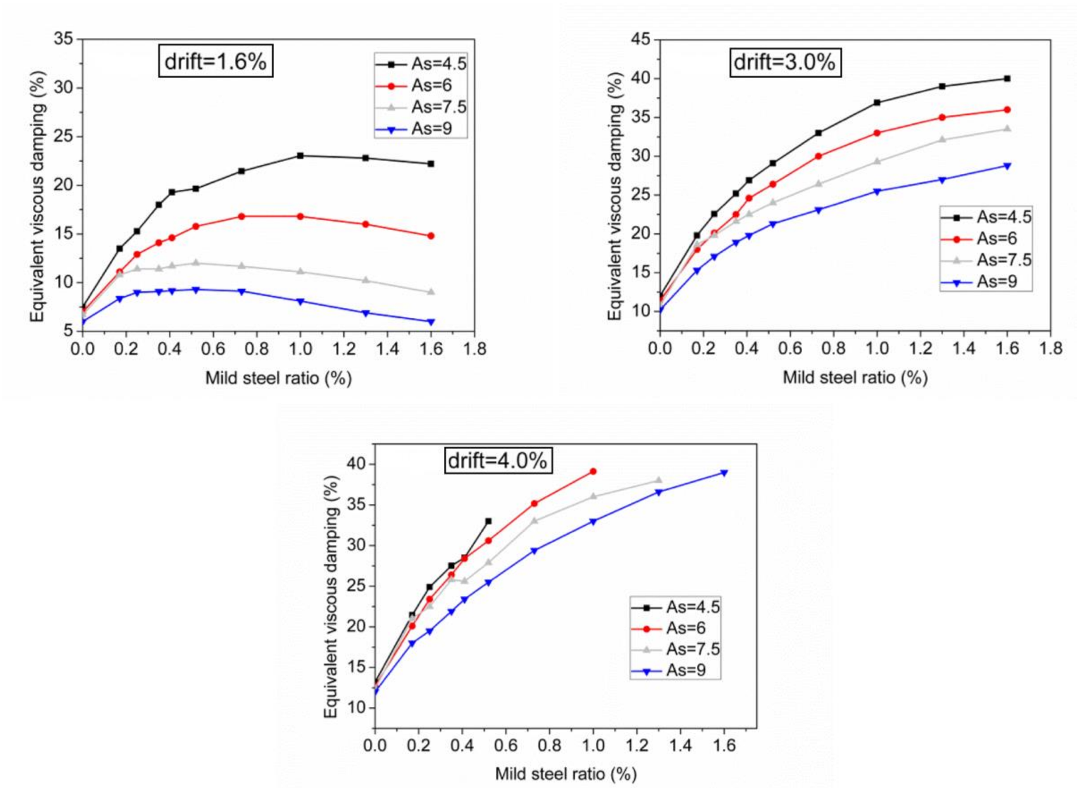

Fig. 22 Effect of mild steel ratio on equivalent viscous damping of precast segmental columns with aspect ratios of 4.5, 6, 7.5 and 9

6. Time-history analysis

In order to examine the dynamic response of precast segmental columns, time-history analysis is conducted. Two earthquake records from Northridge (with 0.41 g) and Loma Prieta (with 0.6 g)

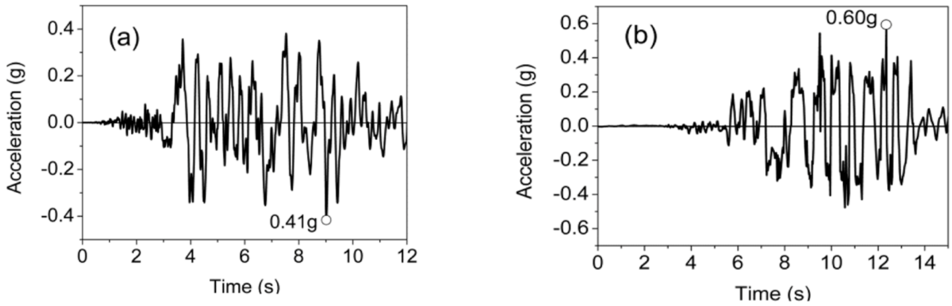

Fig. 23 Earthquake records applied in the analyses: (a) Northridge (b) Loma Prieta

Table 8 Applied earthquake ground motion records. Source: PEER strong motion database

No.	Event	Year	Station	M*[a]	R*[b](km)	PGA(g)	PGA/PGV
1	Northridge	1994	Castaic - Old Ridge Route	6.69	20.7	0.41	0.85
2	Loma Prieta	1989	BRAN	6.93	10.7	0.6	1.14

[a]Moment magnitude
[b]Closest distance to fault rupture

are selected for the analyses. The applied earthquake time-histories are shown in Fig. 23. The characteristics of ground motions are presented in Table 8.

As discussed earlier, the self-centring segmental columns possess low energy dissipation capacity due to the restoration capability of strands during the unloading stages. It is predominantly the segments' opening and low energy dissipation which leads to the high level of peak lateral displacement. In this section, the effect of PT force levels and the continuous mild steel ratio are investigated with regard to lateral peak displacement demand of segmental columns with central PT strands.

For the analysis, a column with four segments, a height of 3.325 m and an aspect ratio of 6.0 is used. A seismic mass of 1000 kN equivalent to the axial superstructure dead load, and one-third of the column's mass is applied. According to the recommendation of AASHTO (1996), a 5.0% damping ratio is applied in the analyses.

6.1 Results and discussion

In Fig. 24, the lateral peak displacement of the segmental column at 40% and 70% initial stress levels are compared under the Northridge earthquake record. The sample with a 70% initial stress level is expected to show close or lower lateral peak displacement due to higher stiffness and strength. Fig. 24(a) compares the lateral responses of the column with 0.41% mild steel ratio at 40% and 70% initial stress. As is shown, this sample at both initial stress levels shows close lateral peak displacements, i.e., the peak lateral top displacement at both initial stress levels is around 113.0 mm. However, in Fig. 24(b), when the continuous mild steel ratio is zero, higher peak lateral displacement is shown at the 70% initial stress level, i.e., 145.9 mm peak lateral displacement versus 118.5 mm at the 40% initial stress level, which is undesirable. In fact, when the initial stress level is 70%, the higher amount of stiffness and strength, alongside an inadequate amount of energy dissipation in the column with 0% mild steel ratio, leads to a concrete crush in the hinge

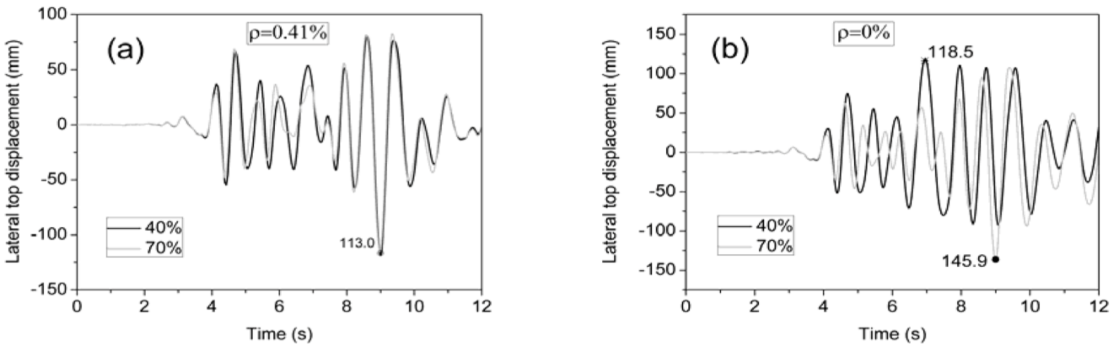

Fig. 24 Lateral seismic response of segmental columns at 40% and 70% initial stress levels under Northridge EQ with mild steel ratios of (a) 0.41% and (b) 0.0%

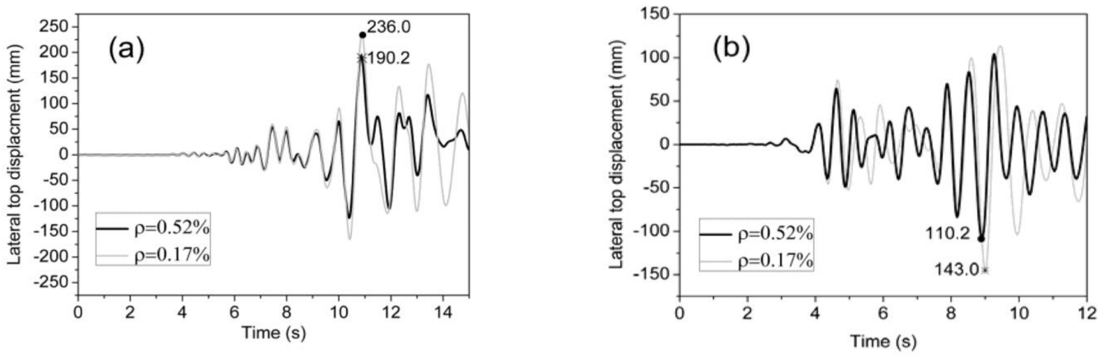

Fig. 25 Effect of mild steel ratio on lateral seismic demand of segmental columns subjected to (a) Loma Prieta and (b) Northridge EQ records

area. This causes considerable stiffness loss, and consequently higher lateral peak displacement.

Fig. 25 compares the lateral peak displacement of the segmental columns with mild steel ratios of 0.17% and 0.52%, subjected to both earthquake ground motions. In Fig. 25(a), under the Loma Prieta earthquake record, the segmental column with a 0.52% steel ratio shows 18% lower lateral peak displacement compared to the columns with a 0.17% mild steel ratio, i.e., 190.2 mm versus 236.0 mm lateral peak displacement of the column with a 0.17% steel ratio. Similar results can be seen in Fig. 25(b) where the column with a 0.52% mild steel ratio shows 23% lower lateral peak displacement under the Northridge earthquake record.

7. Conclusions

Residual displacement, lateral strength, and lateral peak displacement response of precast self-centring segmental columns with low energy dissipation capacity were investigated under nonlinear cyclic and pseudo-dynamic loading. The following conclusions can be made based on experimental and analytical investigations:

1. The segmental columns with strands near the circumference of the cross-section showed

higher stiffness and strength compared to the columns with central strands, but also larger residual displacement. In addition, the column with central strands at a 70% prestressing level showed higher strength compared to a 40% initial stress level, while the columns with strands around the cross-section exhibited similar strength at both 40% and 70% prestressing levels.

2. Increasing the thickness of steel jacket around the first segment corresponded with an increase to the stiffness and strength of the columns. However, it had a little effect on residual displacement and energy dissipation capacity of the self-centring columns. It was shown that large thickness of steel tube jacket might cause excessive stresses in critical areas at large drifts, e.g., the column with a steel tube jacket thickness of 9 mm failed at 3.6% drift due to concrete failure below the steel jacketing areas.

3. The analyses of the segmental columns with aspect ratios of 4.5, 6, 7.5 and 9 indicated that columns with a higher aspect ratio show lower amount of strength and energy dissipation; however, it was shown that aspect ratio has little effect on equivalent viscous damping of the columns.

4. Introducing continuous longitudinal mild steel ratio in higher aspect ratio columns caused lower residual drift and equivalent viscous damping compared to those with lower aspect ratio. It was shown that there is a greater capacity for increasing the amount of mild steel ratio in higher aspect ratio columns until their residual drift exceeds the limitation of 1%. Specifically, the maximum allowed mild steel ratio for the segmental column with aspect ratio of 9.0 was 60% and 23% larger than that of the columns with aspect ratios of 6.0 and 7.5, respectively.

5. Time-history analyses indicated that the columns with inadequate amount of mild steel ratio and higher level of post-tensioning exhibited greater lateral peak displacement response compared to those with higher mild steel ratio and lower post-tensioning level. The column with a 0.52% mild steel ratio showed 19% lower lateral peak displacement compared to that with a 0.17% mild steel ratio under Loma Prieta earthquake record, and displayed 23% lower top displacement under Northridge record.

Acknowledgments

The authors wish to acknowledge the financial support received from the Fundamental Research Grant Scheme of Malaysia (Grant No. FRGS/TK03/UKM/02/4) in connection with this work.

References

AASHTO (1996), *Standard specifications for buildings, 16th edition*, Washington, D.C.

ANSYS, User's manual (2012), Theory reference for the mechanical APDL and mechanical applications.

Bu, Z.Y. and Ou, Y.C. (2013), "Simplified analytical pushover method for precast segmental concrete bridge columns", *Adv. Struct. Eng.*, **16**(5), 805-822.

Caltrans seismic design criteria (1999), California department of transportation.

Chou, C.C., Chang, H.J. and Hewes, J. (2013), "Two dimensional finite element models for post-tensioned precast concrete segmental bridge columns", *Eng. Struct.*, **46**, 205-217.

Chou, C.C. and Hsu, C.P. (2008), "Hysteretic model development and seismic response of unbonded post-tensioned precast CFT segmental bridge columns", *Earthq. Eng. Struct. Dyn.*, **37**(6), 899-921.

Dawood, H., Elgawady, M. and Hewes, J. (2012), "Behaviour of segmental posttensioned bridge piers under

lateral loads", *J. Bridge Eng*., **17**(5), 735-746.
Desayi, P. and Krishnan, S. (1964), "Equation for the stress-strain curve of concrete", *J. Am. Concrete Inst*., **61**(3), 345-350.
Elgawady, M.A. and Dawood, H.M. (2012), "Analysis of segmental piers consisted of concrete filled FRP tubes", *Eng. Struct.*, **38**, 142-152.
Elgawady, M.A. and Sha'lan, A. (2011), "Seismic behaviour of self-centring precast segmental bridge bents", *J. Bridge Eng.*, **16**(3), 328-339.
Hewes, J.T. and Priestley, M.J.N. (2002), "Seismic design and performance of precast segmental bridge columns", PhD. Thesis, University of California, Sandiego.
Japan Road Association (2002), "Design specification of highway bridges. Part V: Seismic design", Japan.
Jeong, H.I., Sakai, J. and Mahin, S. (2008), "Shaking table test and numerical investigation of self-centring reinforced concrete bridge columns", *PEER Report, Pacific Earthquake Engineering*, University California, Berkley.
Kim, T.H., Lee, H.M., Kim, Y.J. and Shin, H.M. (2010), "Performance assessment of precast concrete segmental bridge columns with a shear resistant connecting structure", *Eng. Struct*., **32**(5), 1292-1303
Kwan, W.P. and Billington, S.L. (2003), "Unbonded posttensioned concrete bridge piers I: monotonic and cyclic analyses", *J. Bridge Eng*., **8**(2), 92-101.
Nikbakht, E., Rashid, K., Hejazi, F. and Osman, S.A. (2014), "Application of shape memory alloy bars in self-centring precast segmental columns as seismic resistance", *Struct. Infrastruct. Eng*., DOI:10.1080/15732479.2013.876056.
Ou, Y.C., Chiewanichakorn, M., Aref, A.J. and Lee, G.C. (2007), "Seismic performance of segmental precast unbounded post-tensioned concrete bridge columns", *J. Struct. Eng.*, **133**(11), 1636-1674.
Ou, Y.C., Wang, P.H., Tesaei, M.S., Chang, K.C. and Lee, G.C. (2010), "Large scale experimental study of precast segmental unbonded posttensioned concrete bridge columns for seismic regions", *J. Struct. Eng.*, **136**(3), 255-264.
PEER, Pacific Earthquake Engineering Research centre, University of California, Berkeley.
Priestley, M.J.N., Seible, F. and Calvi, G.M. (1996), *Seismic design and retrofit of bridges*, Wiley, New York.
Sakai, J. and Mahin, S. (2004), "Mitigation of residual displacement of circular reinforced concrete bridge columns", *Proceeding of the Earthquake engineering Conference Vancouver, B.C.*, Canada.
Stanton, J., Stone, W. and Cheok, G.C. (1998), "A hybrid reinforced precast frame for seismic regions", *PCI J*., **42**(2), 20-32.
Stone, W.C., Cheok, G.S. and Stantone, J.F. (1995), "Performance of hybrid moment-resisting precast beam-column concrete connection subjected to cyclic loading", *ACI Struct. J*., **91**(2), 229-249.

CC